SUPPORTING INFORMATION

Chimeric negative regulation of p14ARF and TBX1 induced by a 9p21;22q11.2 translocation associated with melanoma, deafness and DNA repair deficiency

Xiaohui Tan, Sarah Anzick, Sikandar G. Khan, Takahiro Ueda, Gary Stone,
John J. DiGiovanna, Deborah Tamura, Daniel Wattendorf, David Busch,
Carmen Brewer, Christopher Zalewski, John A Butman, Andrew J. Griffith, Paul Meltzer, and Kenneth H. Kraemer

TABLE OF CONTENTS:

Supp. Figure S12. Normal expression of p16 in DD129BE cells.

Supp. Figure S13. Expression of selected genes on chromosome 22 and genes related to *TBX1*.

Supp. Table S1. Results of FISH analysis

Supp. Table S2. Primers for the amplification of chimeric genomic DNA and cDNA

Supp. Table S3. Clinical and laboratory abnormalities in patient DD129BE

Supp. Table S4. Translocations on PATRR22

SUPP. MATERIALS AND METHODS

Ethics Statement

This study was approved by the National Cancer Institute Institutional Review Board, protocol 99-C-0099.

Cultured cells

Fibroblast and lymphoblast cultures from patient (DD129BE/ GM16737), his mother (GM16733, GM16732A), father (GM16735, GM16734A) and normal fibroblasts (AG13145, AG13354) and lymphoblast (GM00130) were obtained from the Human Genetic Mutant Cell Repository (Camden, NJ, USA).

FISH

For whole chromosome painting of chromosomes 9 and 22, hybridizations with individual whole chromosome painting probes labeled with single fluorochromes were used as previously described (Padilla-Nash et al., 2006). To examine translocation on chromosome 9, FISH analysis was performed using a commercial p16/CEP 9 Probe (Vysis™) (Supp. Figure S1). Probes are listed in Supp. Table S1.

Flow sorting and aCGH

The derivative chromosomes 9 and 22 were flow sorted as described previously(Stanyon and Stone, 2008). For aCGH, the sorted chromosomes were amplified using the GenomePlex Single Cell Whole Genome Amplification Kit, WGA4 (Sigma-Aldrich, St. Louis, MO) and following the protocol of the manufacturer. The amplified products were purified using Qiagen PCR purification kit (Qiagen, Valencia, CA) and used as template DNA for array CGH.

For aCGH hybridizations using whole genomic DNA, 900 ng of sample DNA and 900 ng DNA from a reference control (female gDNA, Promega, UK) was digested using AluI and Rsa1 restriction enzymes (Invitrogen, Grand Island, NY), labeled with Cy3-dUTP (sample) and Cy5-dUTP (reference) dyes (Amersham GE Healthcare Bio-Sciences, Piscataway, NJ), purified using a Vivaspin concentrator (Sartorius, Germany), and hybridized to Human

Genome CGH 105A oligonucleotide arrays (Agilent Technologies, Santa Clara, CA) essentially as described previously (Anzick et al., 2010). For aCGH hybridizations using flow sorted WGA DNA, 900 ng of each WGA4 sample was labeled as described above and hybridized with 900 ng of reference gDNA. Fine mapping of the breakpoints was performed using a custom oligonucleotide tiling array covering the genomic intervals chr22:18686076-19210439 and chr9:21692941-22095210 (hg18; NCBI 36.1). The custom tiling array was designed using Agilent's eArray design (Agilent Technologies, Santa Clara, CA). Repetitive sequences were excluded from the tiling array design.

PCR Amplification and sequencing of breakpoint junctions

PCR was used to identify the t(9;22) junction from both the der (9) and der(22) chromosomes using genomic DNA. The PCR products were either sequenced directly or after cloning into pCR4-TOPO vector SURE strain (Stratagene) to maintain unstable inserts.

Analysis of Fusion Transcript

Total RNA extracted from DD129BE fibroblasts was reverse transcribed into cDNA and used as template for PCR amplification of the fusion breakpoint. Primers were designed to flank the probable breakpoints within *CDKN2A* and a hypothetical gene supported by BC039313 (LOC653203) mRNA (Supp. Table S2). PCR was subjected to 34 cycles of PCR using the following conditions: denaturation at 94°C for 1 minute, annealing at 57-65°C for 30 seconds, and extension at 72°C for 45-60 seconds. The amplification products were sequenced.

3′RACE assay.

First strand cDNA synthesis was initiated at the poly(A) tail of mRNA using the adapter primer (AP). Amplification was performed using GSPs located within the p14ARF and LOC653203 and universal primers (UAP). The abridged universal amplification primer (AUAP) was homologous to the adapter sequence used to prime first strand cDNA synthesis. To generate a specific amplification product, we designed second "nested" GSPs to re-amplify the RACE products.

cDNA microarrays

Two hundred nanograms of total RNA was amplified and biotin-labeled using the Illumina TotalPrep RNA Amplification kit (Ambion Inc., Austin, TX). The biotin-labeled cRNAs were quantitated using RiboGreen RNA Quantitation reagent (Molecular Probes, Eugene, OR) and the manufacturer's protocol. For each hybridization, 750 ng of biotin-labeled cRNA was hybridized to HumanRef-8 v2 Expression Beadchips following the manufacturer's recommended protocol (Illumina, San Diego, CA). Arrays were scanned using the Illumina chip scanner and scanned images were processed and analyzed using Bead Studio (Illumina, San Diego, CA).

Laser-capture microdissection (LCM) and Mutation and SNP analysis

Laser-capture microdissection was performed by use of an Arcturus PixCell II microscope (Arcturus Engineering) to separate melanoma cells from normal cells as described(Wang et al., 2009). DNA was extracted using PicoPure DNA Extraction Kit as per the manufacturer's protocol (Arcturus Engineering). Exon sequences of both *p14ARF* and *p16INK4a* were PCR amplified and sequenced. We screened mutations in the entire coding and promoter regions of *CDKN2A* (*p14ARF and p16INK4a*) and three isoforms of *TBX1* by PCR amplification followed by direct genomic sequencing. Primer sequences are available on request.

Host cell reactivation assay

DNA repair capability of DD129BE cells was assessed using post-UV host cell reactivation (HCR) with the pCMVLuc reporter gene plasmid as described previously (Khan et al., 2002). Transient plasmid HCR assay was used to measure functional correction of the *p14ARF* DNA repair defects by the full-length wild-type *p14ARF* cDNA plasmid (*p14ARF*-pEGFP-N1, a generous gift from Dr. A. Fornace) and the known XP complementation groups (*XPA, XPB, XPC, XPD, XPF, XPG*) as well as *ERCC6, cyclin H, p62, p52, p44, p34*, and *MAT*. Briefly, 4 µl (200 ng) of CsCl-purified pCMVLuc, either UV-irradiated (1000 J/m^2) or unirradiated were co-transfected with 0.4 µl (200 ng) of *p14ARF*-pEGFP-N1 effector plasmids into cells using Lipofectamine 2000 (Invitrogen). To estimate the DNA repair capacity after knockdown of the chimeric RNA by siRNA, we co-transfected

pCMVLuc with 20 nmol of siRNA. Relative luciferase activities are presented as a percentage of activities obtained with UV-irradiated versus unirradiated control plasmids.

UV irradiation

Cells were seeded in 10 cm dishes at a concentration of 8×10^5 cells/dish. After a 24 h pre-incubation period, cells were exposed to 10 J/m^2 of UVC (254 nm) and allowed to recover for 6, and 24 h(Khan et al., 2002).

QRT–PCR

Quantification of *TBX1* expression was performed on cDNA using predesigned TaqMan Gene Expression Assays for *TBX1* and beta-actin (*ACTB*) following the manufacturer's protocol (Applied Biosystems by Life Technologies, Carlsbad, CA). *ACTB* was used as the endogenous control and all assays were run in triplicate. Real-time PCR assay for other genes were carried out on a Bio-Rad iCycler iQ system (Bio-Rad, Hercules, CA, USA) using SYBR Green as the fluorescence reporter as described (Khan et al., 2002). Gene expression values were calculated using the ΔΔCt method in which normal fibroblasts were as the calibrator sample. Primers sequences are available on request.

Proteasome Inhibitor MG-132 Assay and Western blotting

For examination of p14ARF protein level in DD129BE, cells were treated with 10 nM MG-132 (Calbiochem, La Jolla, CA) or 0.1% DMSO for 6 h and proteins were extracted for Western blot analysis (Magro et al., 2004). The following antibodies were used: rabbit anti-p14ARF (Novus, NB110-59085, 1:100), rabbit anti-TBX1 (Abcam, ab84730, 1:200), rabbit anti-p16 (Cell signaling, #4824, 1:100), mouse anti-p53 (Santa Cruz, sc-98), mouse anti-MDM2 (GeneTex, Inc. GTX16895, 1:800), mouse anti-XPC (ab6264, Abcam, Inc., 1:500), mouse p21 C19-G (sc-397-G, Santa Cruz, 1:100), mouse anti-actin (A5316, Sigma, 1:5000).

Immunofluorescence

Cells were seeded at 2×10^4 cells per well on glass coverslips in six-well plates and fixed in 2% paraformaldehyde as described previously(Dawe et al., 2007). Confocal images were

obtained using a LSM 510 Confocal microscope (Carl Zeiss). The number of nuclei containing at least one localized area of immunofluorescence was determined by examination of the confocal images. Primary rabbit polyclonal or mouse monoclonal antibodies for immunofluorescence were as follows: anti p14 mouse antibody (Novus, NB200-111, 1:200); anti-TBX1 antibody (Abcam, ab18530, 1:200); mouse anti-p53 (Santa Cruz, sc-98, 1:200), mouse anti-MDM2 (GeneTex, Inc. GTX16895, 1:200), Alexa Flour 568 goat anti-mouse IgG (Invitrogen, 1:500); and Alexa Flour 568 goat anti-mouse IgG (Invitrogen, 1:500).

siRNA

siRNAs were purchased from Ambion. Sequences of siRNAs targeted to *p14ARF-FAM230A* are shown in Figure 3c. siRNAs against GAPDH (4390849 and 4390844, Ambion) were used as positive and negative controls). Cells were transfected with 20 nmol of siRNA using Lipofectamine 2000 (Invitrogen).

Statistical analysis

Statistical evaluation was performed using the Student's unpaired t-test. Data are presented as mean $\pm$ s.e.m. and $P \leq 0.05$ was considered statistically significant.

SUPP. RESULTS

A constitutional translocation within 9p21 and 22q11.2

Chromosome analysis of cultured skin fibroblasts and whole chromosome painting identified a balanced translocation between chromosomes 9 and 22 [46, XY, t(9;22)(p22;q11.2)] (Supp. Figure S1a-c). Fluorescent *in* situ hybridization (FISH) analysis localized the breakpoint between D9S1747 and D9S1752 on 9p21 and within LCR22-B on 22q11.2 (Supp. Figure S1d, e and Supp. Table S1). As *TBX1* on chromosome 22 has been identified as a candidate for involvement in the DGS, we paid special attention to the *TBX1* probe. However, this signal was not translocated to der(9) or other chromosomes (Supp. Figure S2c). Array-comparative genome hybridization (aCGH) analysis on whole genomic DNA showed no copy number variations at 9p21 or 22q11.2 (Supp. Figure S3).

Mapping the breakpoints within *CDKN2A* gene on 9p21 and LCR22-B on 22q11.2

We considered the possibility that the negative result of aCGH on whole genomic DNA could reflect a balanced translocation at the resolution of the array. We were able to isolate derivative chromosomes by bivariate flow sorting (Supp. Figure S4a and d). Hybridizing the sorted der(9) and der(22) chromosomes to a tiling array of chromosome 22 and 9 clone sets (Figure 3e and f) narrowed the breakpoint on chromosome 9 to a 2-kb region between *CDKN2A* exons 1β and 1α. The breakpoint on chromosome 22, however, could only be localized approximately to an 890-kb region within the 3-Mb DGCR due to inability to identify the sequences containing LCRs within the gap. These observations suggested that the translocation resulted in a novel rearrangement involving *p14ARF* and LCR22-B.

The breakpoints occurred within AT-rich repeats in *CDKN2A* on chromosome 9 and *PATRR22* on chromosome 22

We next sought to fine-map the breakpoint junction fragment with a PCR-based approach using DNA templates derived from genomic DNA and flow-sorted derivative DNA. The exact junction sequences of der(9) and der(22) were successfully amplified using a large series of primers (Figure 2, Supp. Figure S6 and Supp. Table S2). Both the chromosome 9 and 22 translocation breakpoints were located within short interspersed element (SINE) AT repeat regions. The translocation was almost perfectly balanced with a 4-bp region of overlap (GTAT/ATAC) and deletion of only 67 bp in ATRR flanking the der(9) breakpoint and 76 bp in PATRR22 flanking the der(22) (Figure 2).

The breakpoint occurred in intron 1 of *CDKN2A* on chromosome 9 and in PATRR22 in LCR-B on chromosome 22. We theorized that the t(9;22) breakpoint on chromosome 22 might lie in the same location as t(11;22)(Tapia-Paez et al., 2001) and t(17;22) (Kurahashi et al., 2003). A BLAST search revealed that the region surrounding the PATRR22 (Kurahashi et al., 2007) had 99% identity to a region including the first 5 exons of a predicted gene, *LOC653203*, located approximately 80 kb away from the gap (Supp. Figures S5b, S6a, S7, and S8b). Due to the duplicated-sequence character of LCR-B, we theorized that PATRR22 might lie within a new gene with high homology to *LOC653203* in the gap. This s putative gene was named *FAM230A*

by HUGO (Figure 5). A 5-kb genomic DNA chimeric PCR product including intron 1 of *CDKN2A* on chromosome 9 and intron 1 to 3 of *FAM230A*/*LOC653203* was obtained from DD129BE, but not from the control cells, using long nested PCR (Supp. Figure S9). Our results indicate that the t(9;22) breakpoint on chromosome 22 lies in a similar PATRR22 location to recurrent translocations t(11;22) and t(17;22) (Supp. Table S4 and Supp. Figure S8) within the new gene, *FAM230A* (GenBank accession number: JX456222).

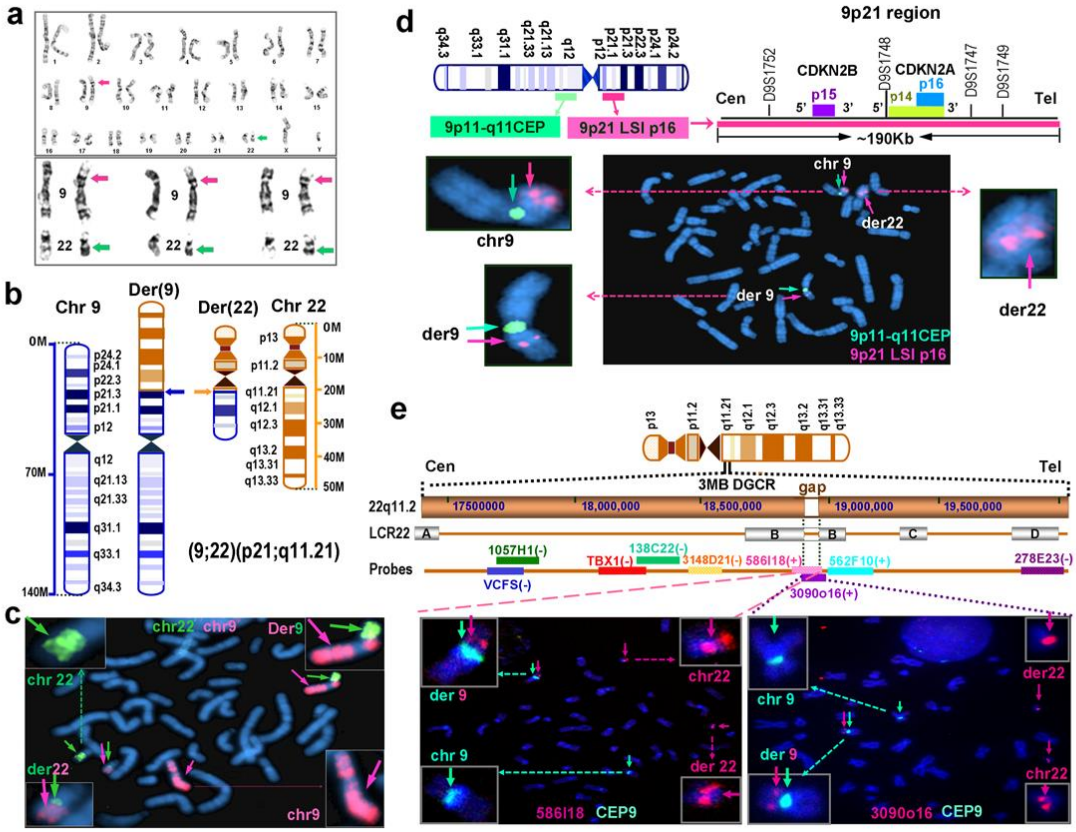

Supp. Figure S1. Karyotype and FISH analyses of t(9; 22) in patient DD129BE. (a) Representative metaphase chromosomes of normal and derivative chromosomes 9 and 22. (b) Ideogram of normal and derivative 9 and 22 chromosomes. Arrows indicate the locations of breakpoints on chromosomes. (c) The hybridization of whole chromosome painting probe of chromosome 9 (red) and chromosome 22 (green) revealed that part of chromosome 9p was translocated onto chromosome 22q. (d) Mapping the chromosome 9 breakpoint by p16 probe (red). At the top is the relative position of centromeric probe CEP9 and LSI p16 probe on chromosome 9. A centromeric probe CEP9 (co-hybridized in green) is used as a control. The LSI p16 probe spans the breakpoint on chromosome 9 showing signals on normal 9, der9, and der22. (e) Mapping chromosome 22 breakpoint by multiple probes in the 3Mb DGCR. At the top is the relative position of BAC probes used in FISH experiments. Probes split in the metaphase spreads are indicated by (+) while those that are not split are indicated by (-).RP11-586I18, RP11-3090o16 and RP11-562F10 were split by the breakpoint on chromosome 22. A centromeric probe CEP9 (cohybridized in green) is used as a control.

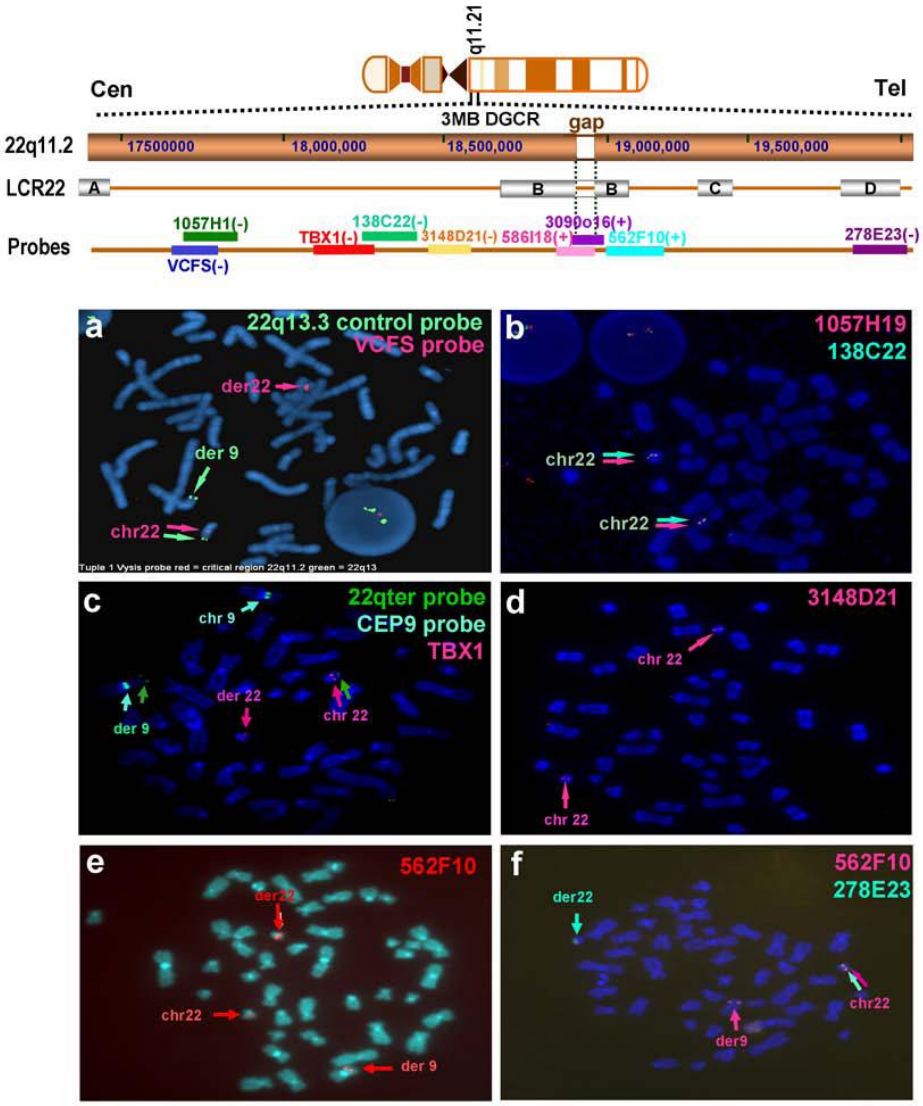

Supp. Figure S2. Mapping chromosome 22 breakpoint by multiple probes in the 3Mb DGCR. At the top is the relative position of BAC probes used in FISH experiments. Probes split in the metaphase spreads are indicated by (+) while those that are not split are indicated by (-).Probe VCFS (a), RP11-1057H19 and RP11-138C22(b), TBX1 (c), CTD-3148D21(d) and RP11-278E23 were not split by the breakpoint on chromosome 22 while RP11-562F10 was split by the breakpoint on chromosome 22.

A

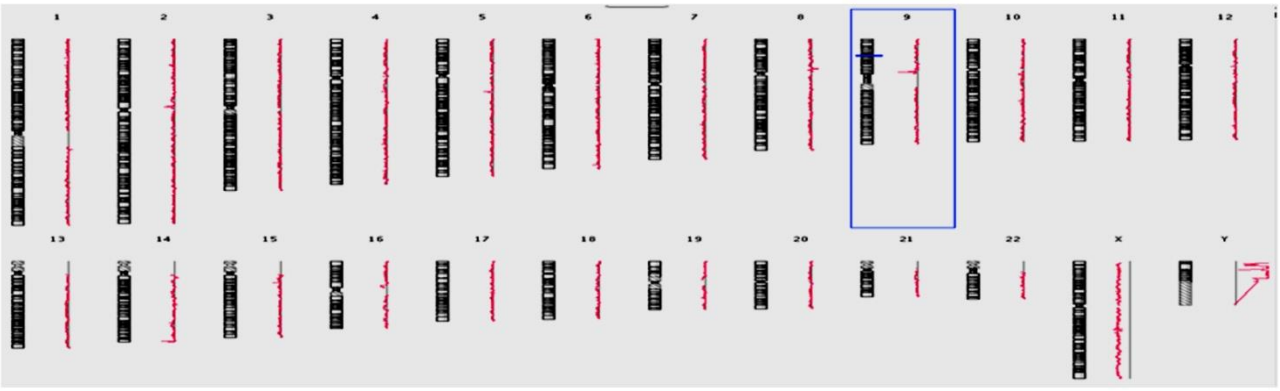

B Chromosome 9

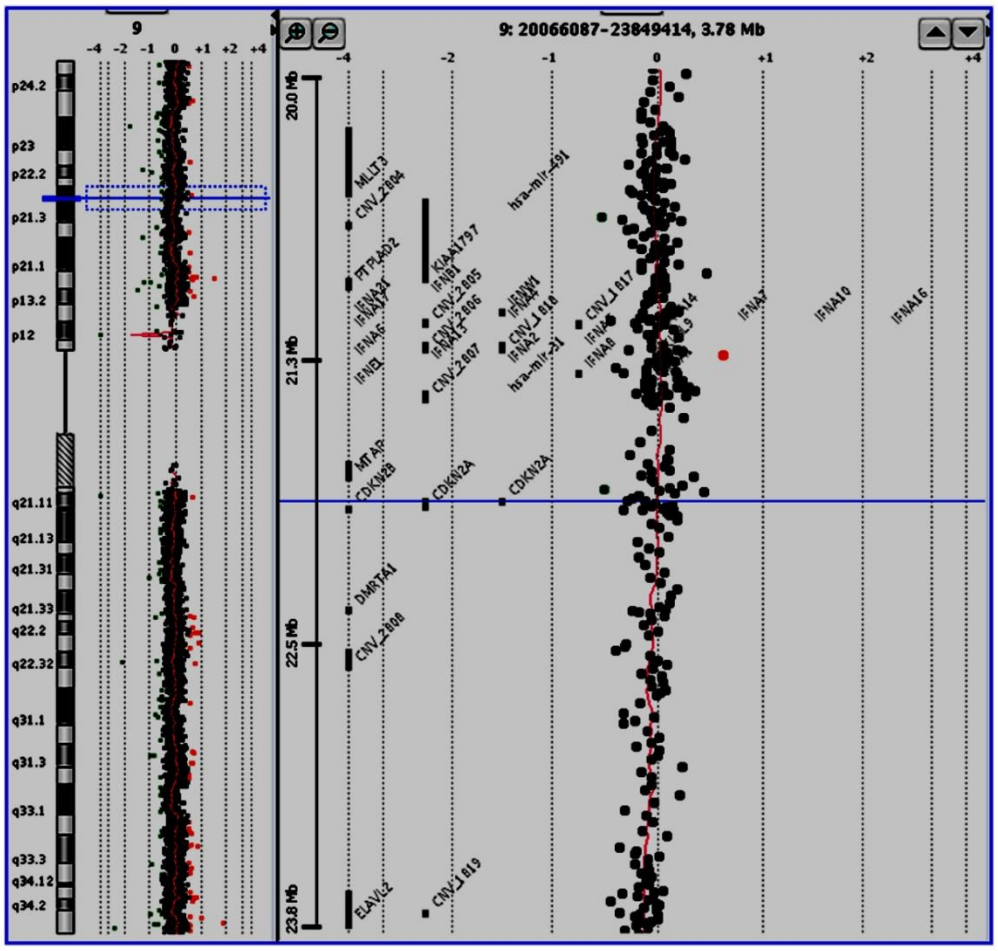

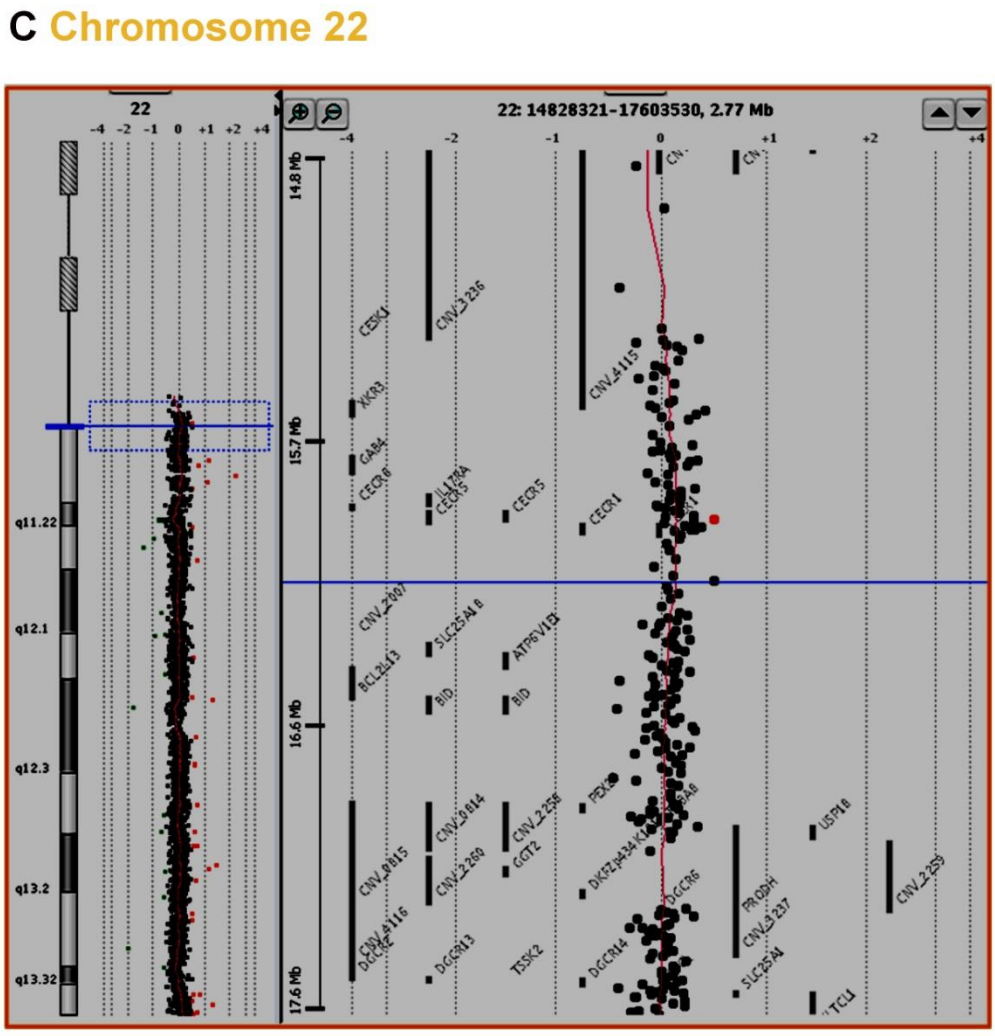

Supp. Figure S3. Array CGH profiles of the genomic DNA from patient DD129BE shows a normal pattern (a) without evidence of copy number variations or translocation on chromosomes 9 (b) and 22 (c).

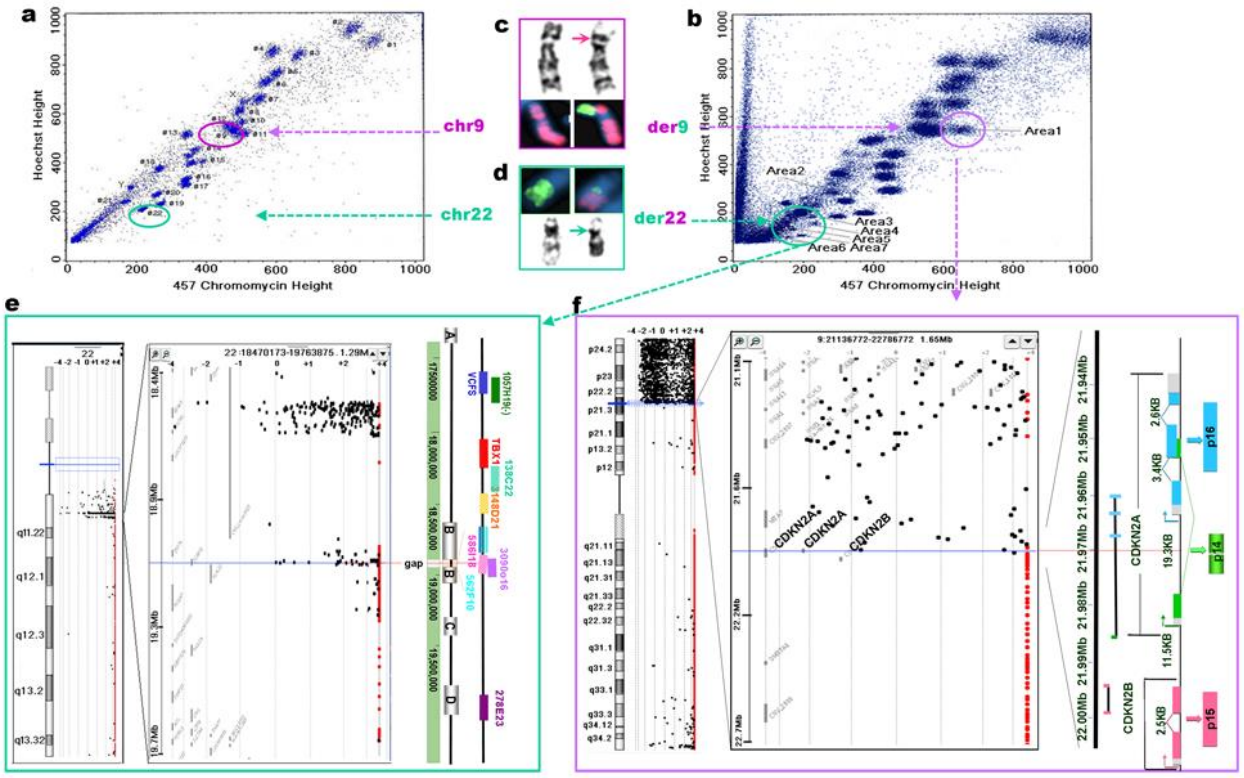

Supp. Figure S4. Analysis of t(9;22) in patient DD129BE. Chromosomes from the normal (a) and patient (b) lymphoblastoid cell lines were isolated by chromosome sorting. (c) Karyotype (upper row) and whole chromosome painting (lower row) of chromosome 9 of DD129BE showing translocation of portion of chromosome 22 to der(9). (d) Karyotype (lower row) and whole chromosome painting (upper row) of chromosome 22 of DD129BE showing translocation of portion of chromosome 9 to der(22). (e and f) Flow-sorted DNA from chromosomes 22 and 9 was hybridized to a high-resolution array CGH with multiple 800 bp fragments for fine mapping of the translocation breakpoint. (e) The breakpoint was mapped to 3 Mb of DGCR on chromosome 22. (f) The breakpoint was mapped to a region of 2Kb in intron 1 of *CDKN2A* gene on chromosome 9.

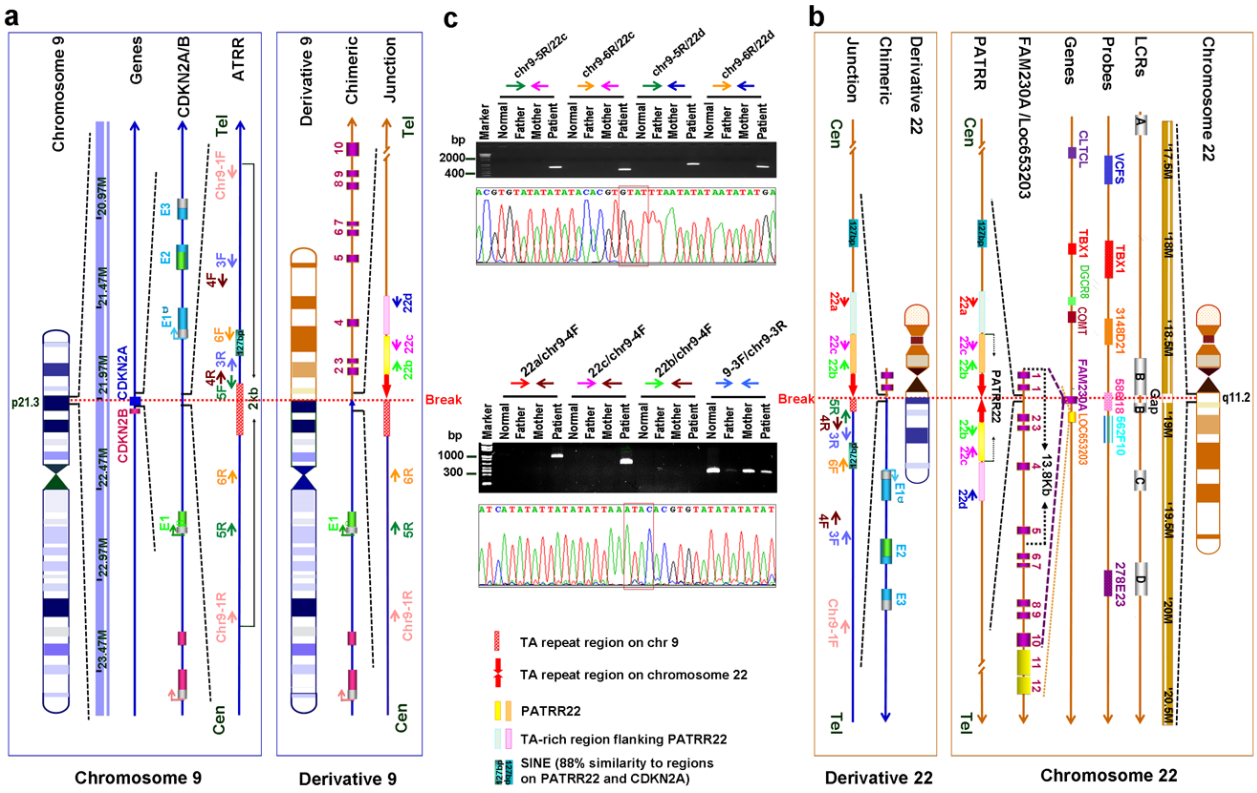

Supp. Figure S5. Molecular cloning and characterization of t(9;22) junction fragments in patient DD129BE by PCR. On chromosome 9, primers were designed within the 2 Kb region narrowed by aCGH. On chromosome 22, since the breakpoint was narrowed in LCR22-B by FISH and aCGH, we reasoned that the t(9;22) breakpoint might lie in the translocation hotspot PATRR22. Thus we used primers outside the PATRR22 as described previously. The 9p21region and the 22q11 region are enlarged, represented by navy blue and brown bands respectively with arrows drawn from centromere to telomere. The relative location of the breakpoint is indicated by a dotted red line. Head-to-head red arrows indicate the inverted AT repeat region of PATRR22. Yellow and brown boxes represent relatively non-AT-rich regions in PATRR22. Stippled azure and pink boxes indicate the AT-rich regions flanking the PATRR22. Two 88% homology SINE sequences flanking breakpoints are depicted by navy blue and bluish green boxes. Primer pairs used to PCR amplify are depicted as oppositely directed arrows with colors. (a) A schematic depiction of chromosome 9 and 9p21 structure (left panel) and derivative (9) and junction structure (right panel). (b) Chromosome 22 and normal structure of 3 Mb DGCR (right panel) and derivative 22 (left panel). *FAM230A* (purple) and *LOC653203* (yellow) gene were enlarged. The identical exon sequences of *FAM230A* and *LOC653203* were drawn with purple boxes with yellow frame. The sequences were drawn with purple and yellow for *FAM230A* and LOC653203, respectively. (c) Representative results of PCR for der (9) with sequence of junction fragment of der(9) (top) and der(22) (bottom). Both the chromosome 9 and 22 translocation breakpoints were located within short interspersed element (SINE) AT repeat regions. The translocation was almost perfectly balanced with a 4 bp region of overlap (GTAT/ATAC, in the red box) and deletion of only 71 bp in ATRR flanking the der(9) breakpoint (Figure 2).

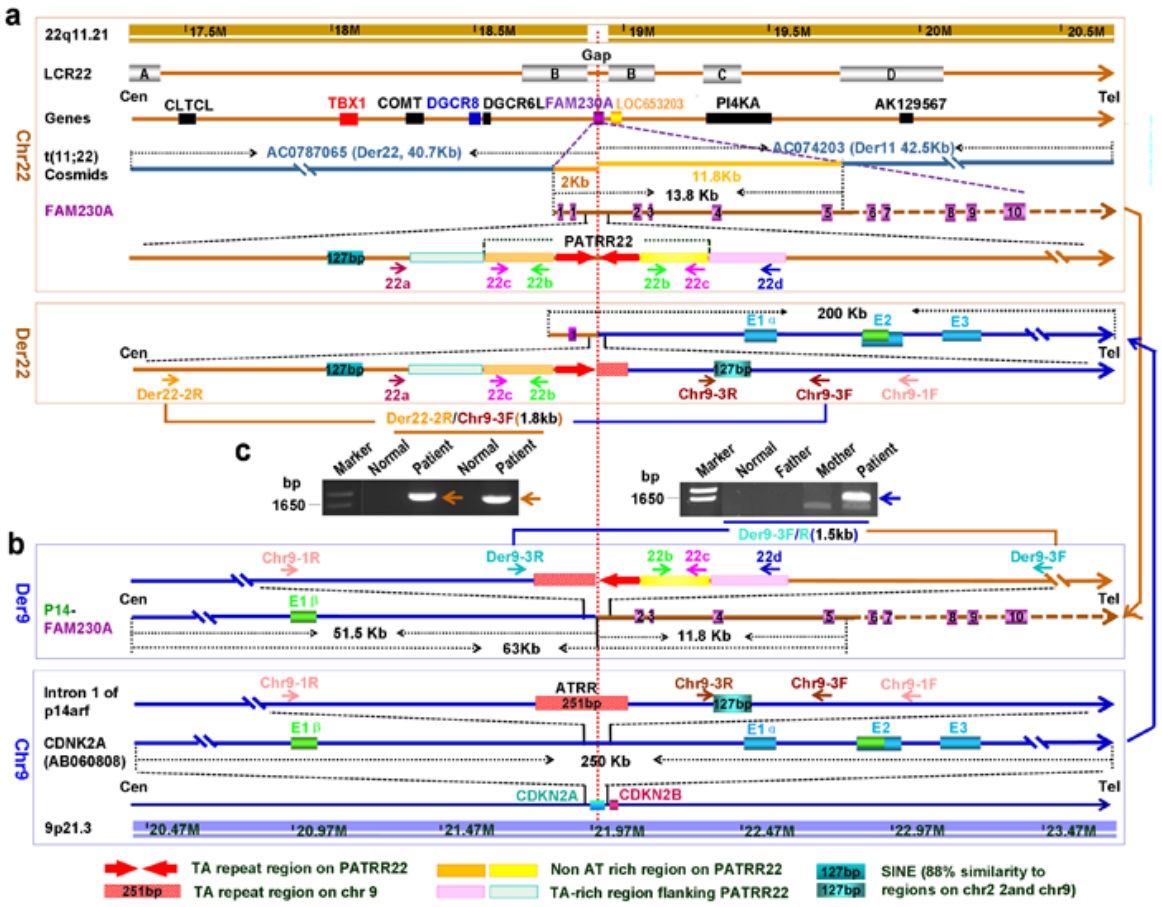

Supp. Figure S6. Cloning of larger der(9) and der(22) junction fragments surrounding PATRR22. To extend the sequence surrounding the breakpoint on PATRR22, the putative 13.8 Kb sequence encompassing PATRR22 was inferred from clones including t(11;22) junctions (cos4: AC074203 and cos6: AC087065). (a) A schematic depiction of normal and derivative 22 surrounding the breakpoint represented by the brown arrows drawn from centromere (left) to telomere (right). The upper panel shows normal structure of 3Mb DGCR, whereas the lower panel indicates der(22) structure. The relative locations of the breakpoints are indicated with a dotted red line. Head-to-head red arrows indicate the inverted AT repeat region of PATRR22. Yellow and brown shading represents relatively non-AT-rich regions in PATRR22. The light blue and pink boxes indicate the AT-rich regions flanking the PATRR22. Primer pairs used to PCR amplify are depicted as oppositely directed arrows with colors. (b) A schematic depiction of the structure of the region surrounding the breakpoint on chromosome 9 represented by the blue arrows drawn from centromere (left) to telomere (right). The upper panel shows the structure of chimeric *p14ARF-FAM230A* on der(9), the lower panel indicates normal *CDKN2A* structure. We reconstructed a 63-Kb der(9) sequence by combining upstream sequence of *CDNK2A* gene (AB060808) (upstream from the der(9) breakpoint) and the distal sequence of the putative chromosome 22 (distal sequence of the der (22) breakpoint), with a 200Kb der (22) sequence by combining downstream sequence of *CDNK2A* gene (AB060808) and proximal sequence of the

putative chromosome 22 (upstream from der (22) breakpoint). (c) Representative results of PCR for der (22) (left) and der(9) (right) from DD129BE cells using conventional PCR. Left panel: Referring to the putative der(22) sequence. By using the primers in the 2 Kb breakpoint region on chromosome 9 and in the 13.8 Kb putative sequence on chromosome 22, we cloned a ~1.5 kb der(22) junction PCR product encompassing the 989 bp chromosome 22 sequence containing the proximal half of PATRR22 region followed by an extra AATA and 475 bp chromosome 9 sequence utilizing proximal primers on chromosome 22 (989 bp away from the der(22) breakpoint) and distal primers on chromosome 9. PCR was performed at 94°C for 45 sec, 60°C for 45 sec, and 72°C for 45sec. Right panel: Representative results of PCR products of der(9). Referring to the putative der(9) sequence, we cloned a 1.4kb der(9) junction PCR product utilizing proximal PCR primers on chromosome 9 and distal primers on chromosome 22 from genomic DNA of the patient DD129BE.

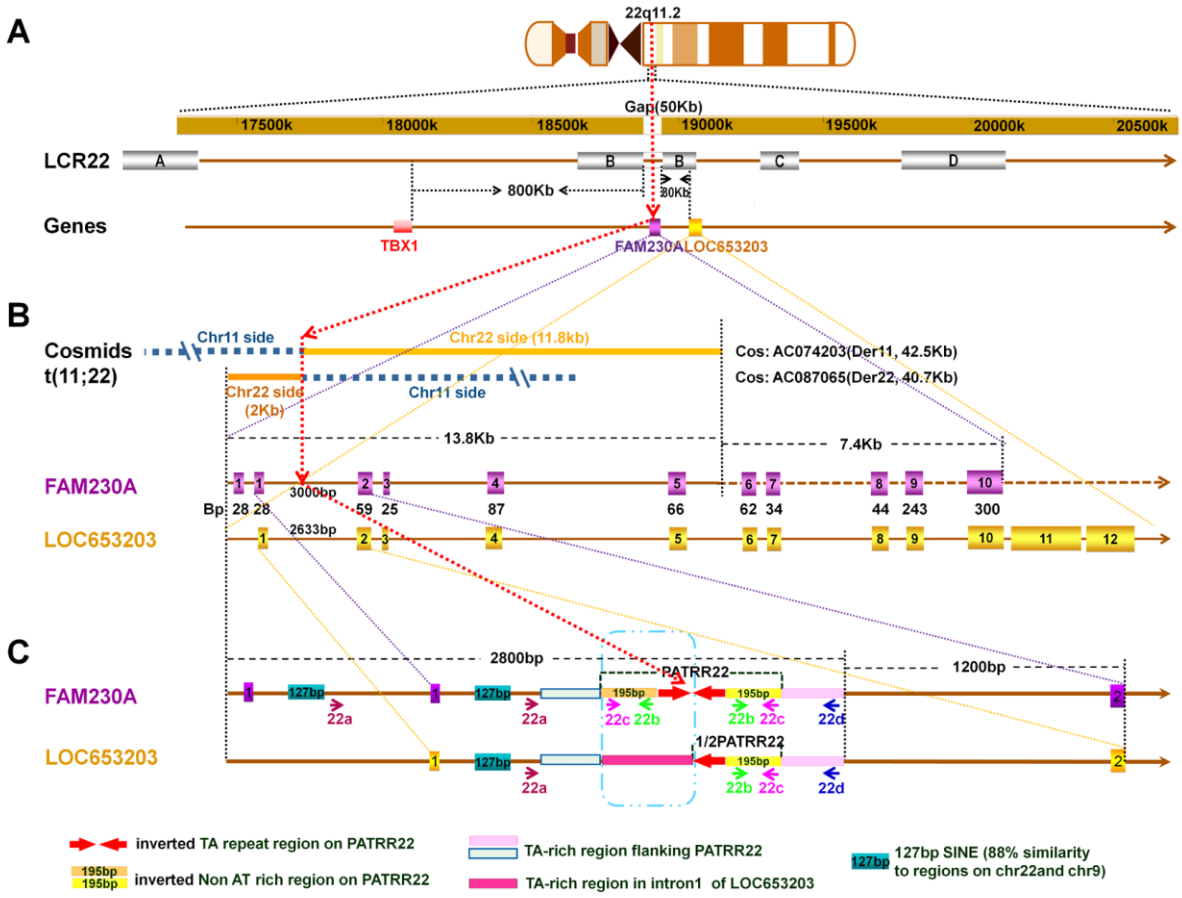

Supp. Figure S7. Comparison of *FAM230A* and *LOC653203* within 3Mb DGCR on 22q11.2. A. Location of *FAM230A* within the gap on chromosome 22: 80 kb from *LOC653203* and 800kb from *TBX1*. The location of the translocation breakpoint is indicated by dotted red arrows. B. Two cosmids AC087065 (der(22)) and AC074203 (der(11)) are indicated by bold lines in which the chromosome 22 sequences on der(11) are indicated in orange, sequences on der(22) in yellow, and sequences on chromosome11 indicated in blue. C. *FAM230A* and *LOC653203* are indicated by purple and yellow, respectively. The size of each exon in base pairs is indicated below the exons on *FAM230A* and *LOC653203*. An entire PATRR22 appears in the first intron of *FAM230A* while a half of PATRR22 appears in the first intron of *LOC653203*. The region that differs between *FAM230A* and *LOC653203* is circled by light blue. In (a), (b) and (c), the arrows with red dotted line indicate the location of breakpoints.

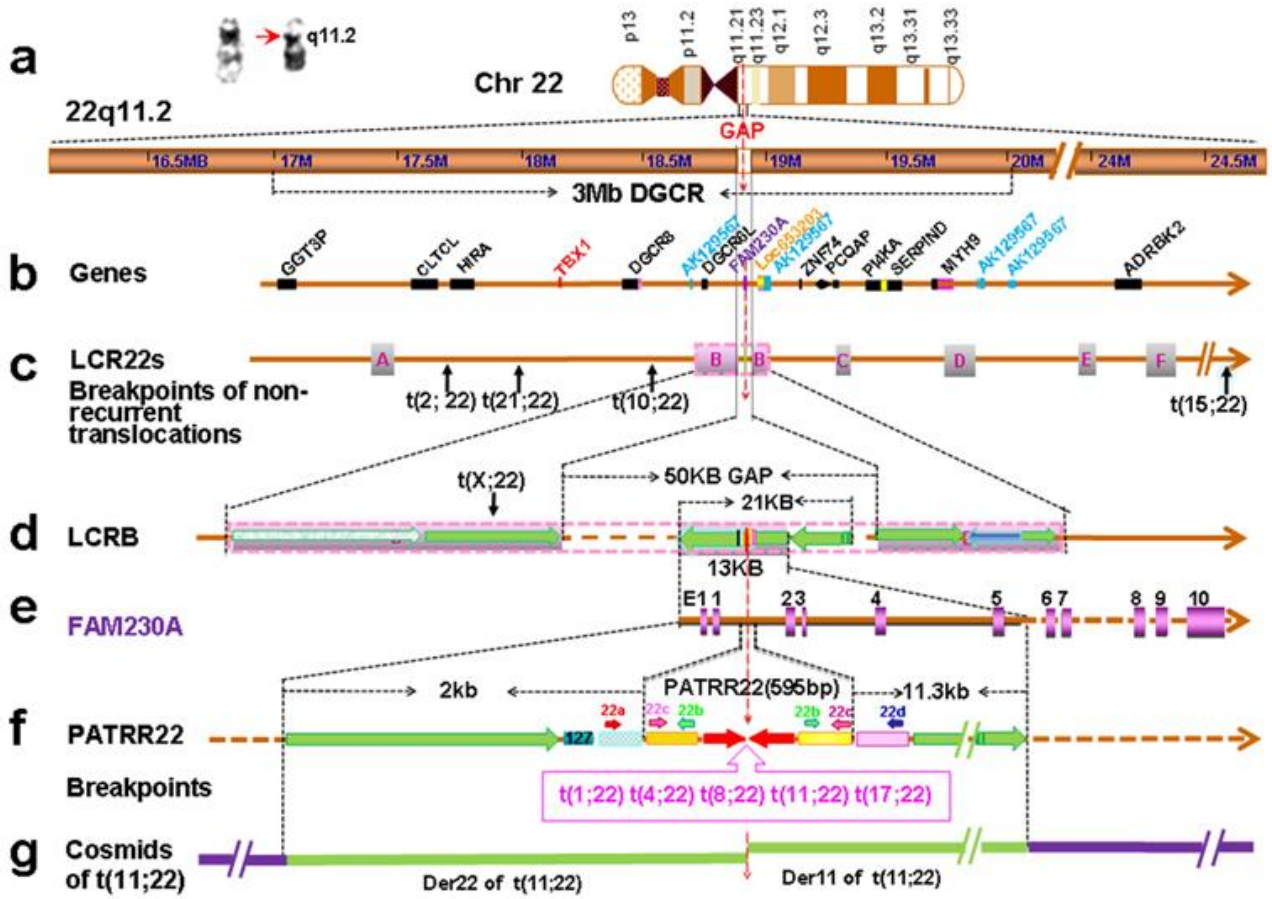

Supp. Figure S8. Extending the known sequence in the unclonable gap on 22q11.2 from 13Kb to 21 Kb. (a) Chromosome 22q11.2 region. (b) Genes in 22q11.2 region. (c) Low copy repeat regions A-F in 22q11.2 region and the locations of breakpoints of non-recurrent translocations (from references (Budarf et al., 1995; Holmes et al., 1997; Debeer et al., 2002; Gotter et al., 2004; Li et al., 2008)). (d) Enlargement of low copy repeat B (LCR22-B). (e) *FAM230A* in the 50Kb gap. (f) PATRR22 in *FAM230A* intron1 and the positions of PATRR22 associated translocation breakpoints (see Supp. Table S3 and references therein) (g) Relative position of *FAM230A* and the t(11;22) breakpoint surrounding sequences on two cosmids(Tapia-Paez et al., 2001). The arrows with red dotted line indicate the location of breakpoint.

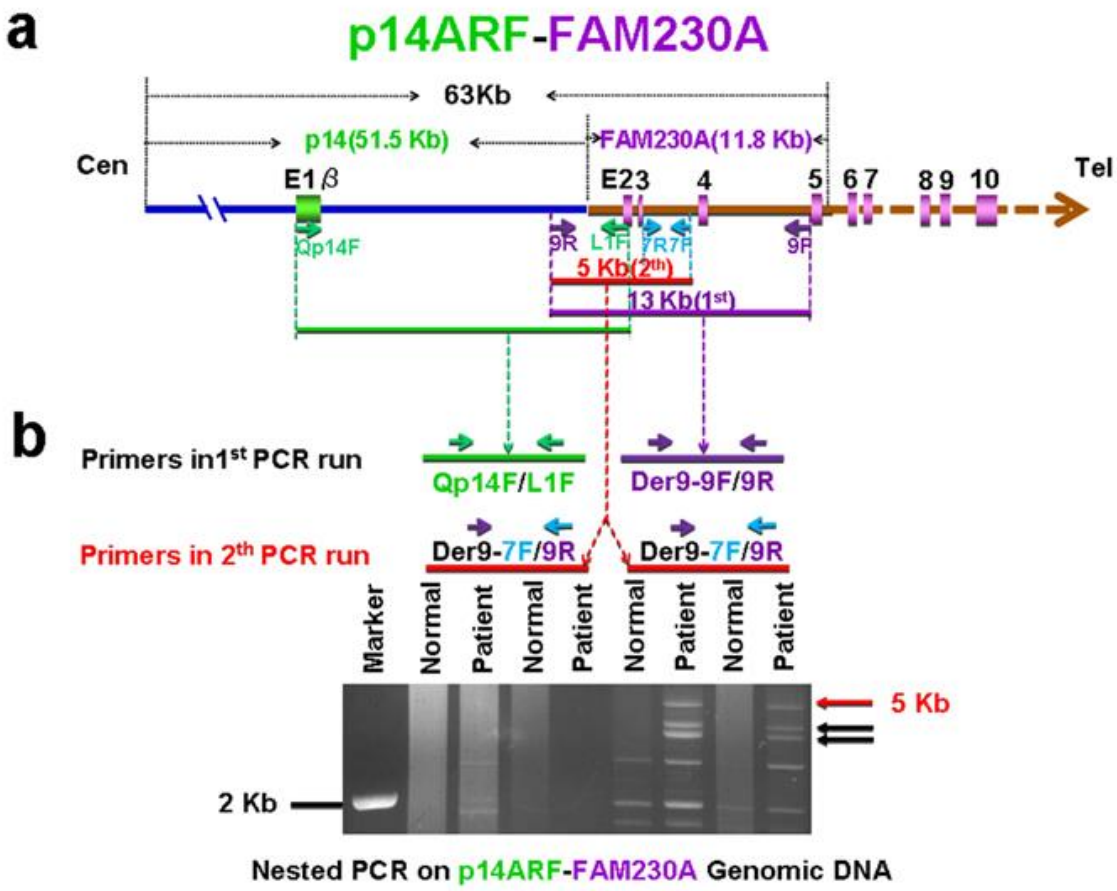

Supp. Figure S9. Cloning of larger der(9) junction fragments surrounding PATRR22 by nested long PCR. (a) A schematic depiction of the chimeric DNA sequence of p14ARF-*FAM230A*. The *p14ARF* and *FAM230A* sequences are shown by blue and brown arrows respectively from centromere to telomere. Exon1 β of *p14ARF* is shown as a green box and the exons on *FAM230A* are shown as purple boxes. Forward and reverse primer pairs are labeled with the same colors. The expected lengths of the PCR products are shown. (b) Agarose gel electrophoresis of PCR amplicons. DNA extracted from patient and normal cells was used as template. Products of the first PCR were subsequently used in a second set of PCR reactions using nested PCR primers to further amplify a portion of the targeted DNA fragment of *p14ARF-FAM230A*. DNA extracted from the tissues was used as template in the PCR. A nested-PCR (second PCR) resulted in DNA bands of an approximate length of 5Kb in DD129BE only with the second set of primers located inside of the primers of 1st PCR run. In contrast, no bands were visualized in the normal cell line. Primers sequences used are shown in Supp. Table S2.

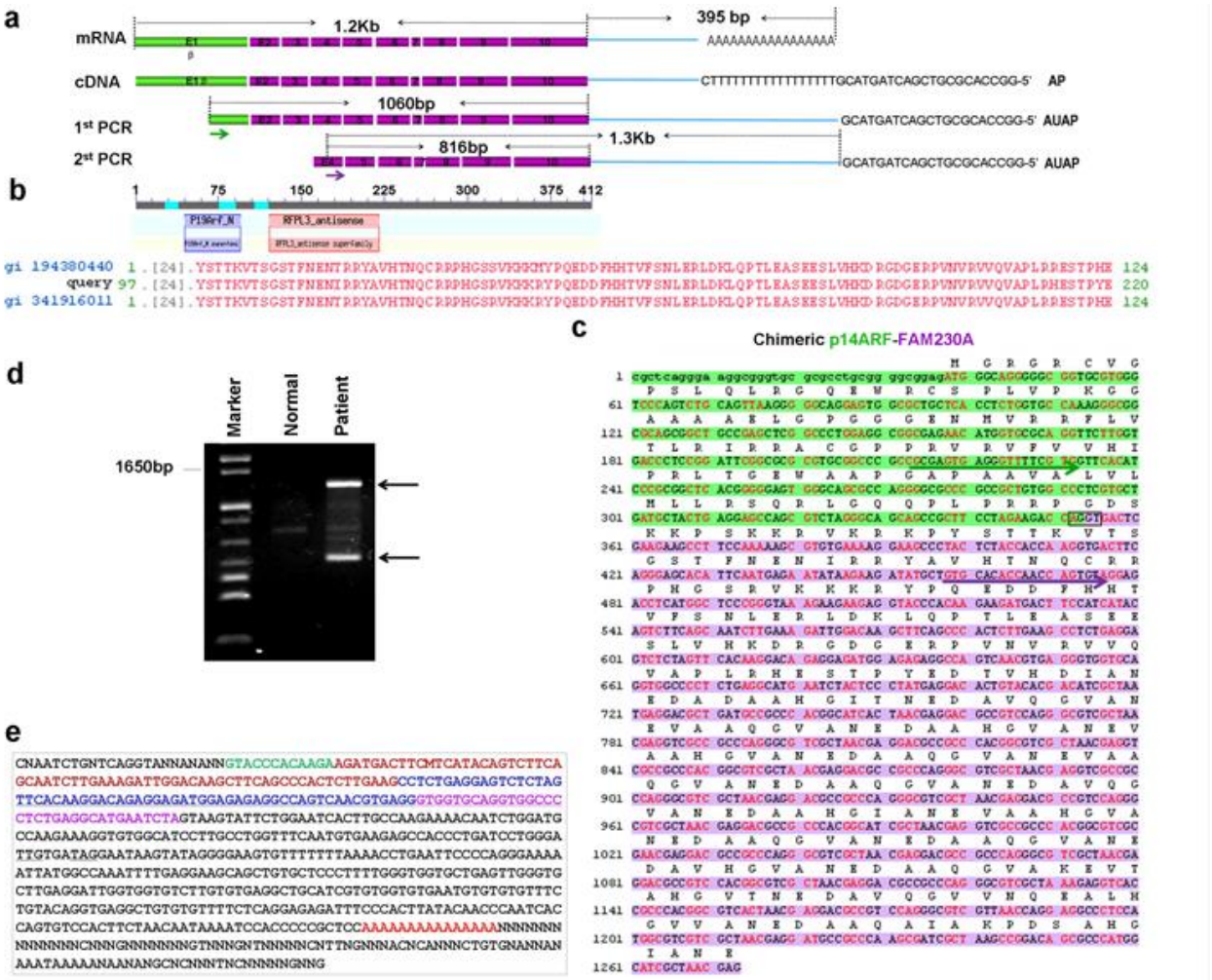

Supp. Figure S10. Identification of 3'UTR sequence of chimeric *p14ARF-FAM230A* by 3'RACE. (a) A schematic depiction of 3'UTR. *CDKN2A* exon1β is indicated by green boxes and *FAM230A* by purple boxes. Small arrows depict the gene specific primers for 3'UTR.The light blue lines represent the untranscribed region. The adapter primer (AP) and abridged universal amplification primer (AUAP) were shown followed the light blue lines (b) The conserved domains in *p14ARF-FAM230A*. A GenBank search revealed that the *p14ARF* portion of the chimeric protein has a high homology with mouse p19arf super family while the amino acids 97 to 220 of DGCR15 have 100 % identity to Superfamily cl11129, ret-finger like protein 3 (RFPL3) antisense (Seroussi et al., 1999; Bonnefont et al., 2008). (c) Nucleotide sequence (1273 bp) and deduced amino acid sequence (411 aa) of chimeric *p14ARF-FAM230A* cDNA. Amino acids are numbered from the initiating start codon methionine (M). *p14ARF* part is in green highlight and the *FAM230A* part is shown in purple highlight. The full sequence was submitted to GenBank (accession no.: JX456220). (d) Agarose gel electrophoresis of 3'UTR amplicons. Due to its highly repetitive sequence multiple PCR products were obtained from DD129BE cells. (e) Representative sequence of the 3'UTR products. The green sequence represents exon 4, the dark red sequence represents exon 5, the blue sequence represents exon 6, the pink sequence represents exon 7. The deduced 412-amino acid sequence contains 395 bp of the 3'-UTR including a stop codon (TGA), polyadenylation signal (AATAAA) and poly(A) tail.

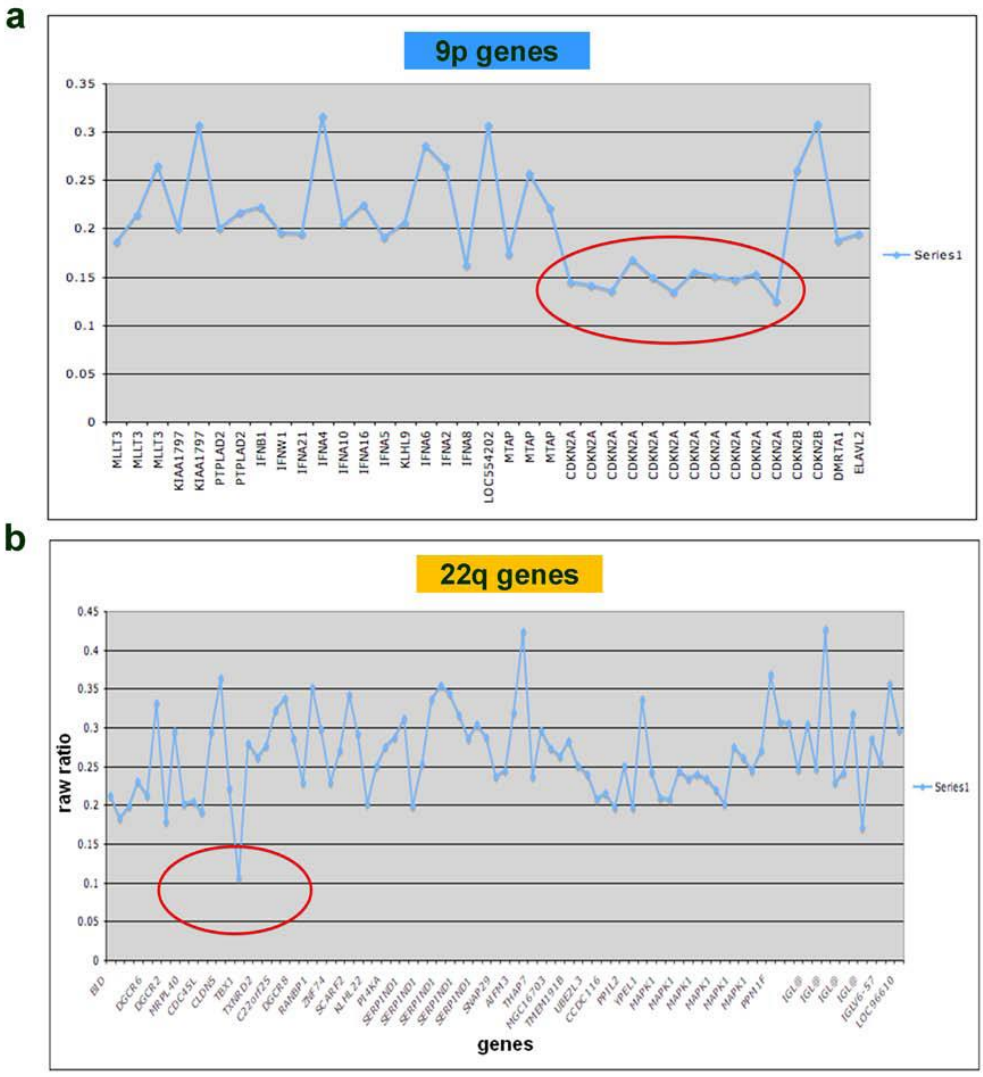

Supp. Figure S11. Global gene expression in DD129BE cells using cDNA microarrays show reduced expression of *p14ARF* and *TBX1*. (a) Genes on chromosome 9p showing low expression of *CDKN2A.* (b) Genes on chromosome 22q showing low expression of *TBX1*.

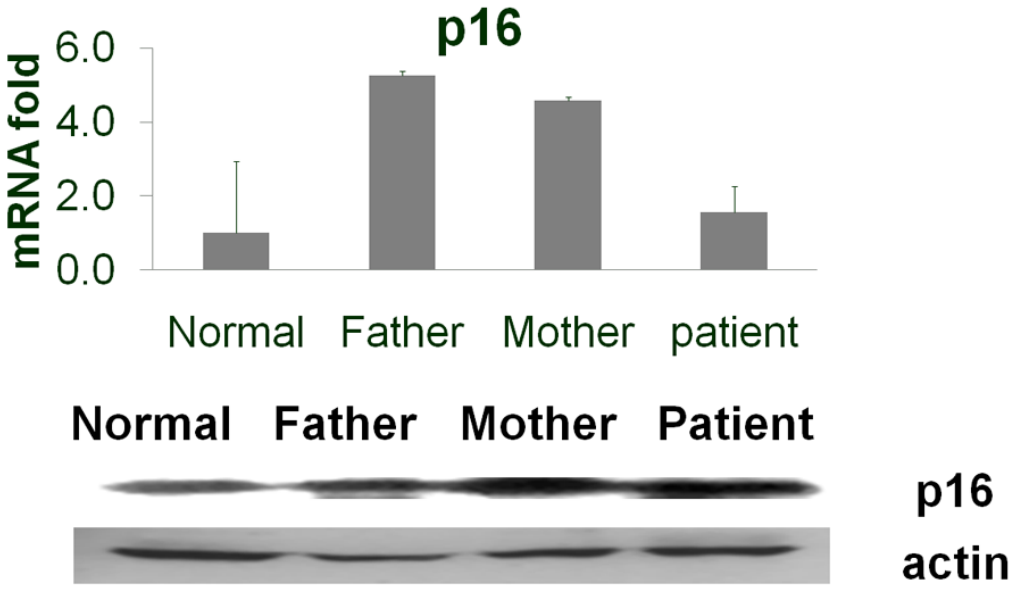

Supp. Figure S12. Normal expression of p16 in DD129BE cells. (a) QRT-PCR showing relative expression of *p16INK4a* mRNA. (b) Western blot of p16 protein in cells from normal, mother, father and patient DD129BE.

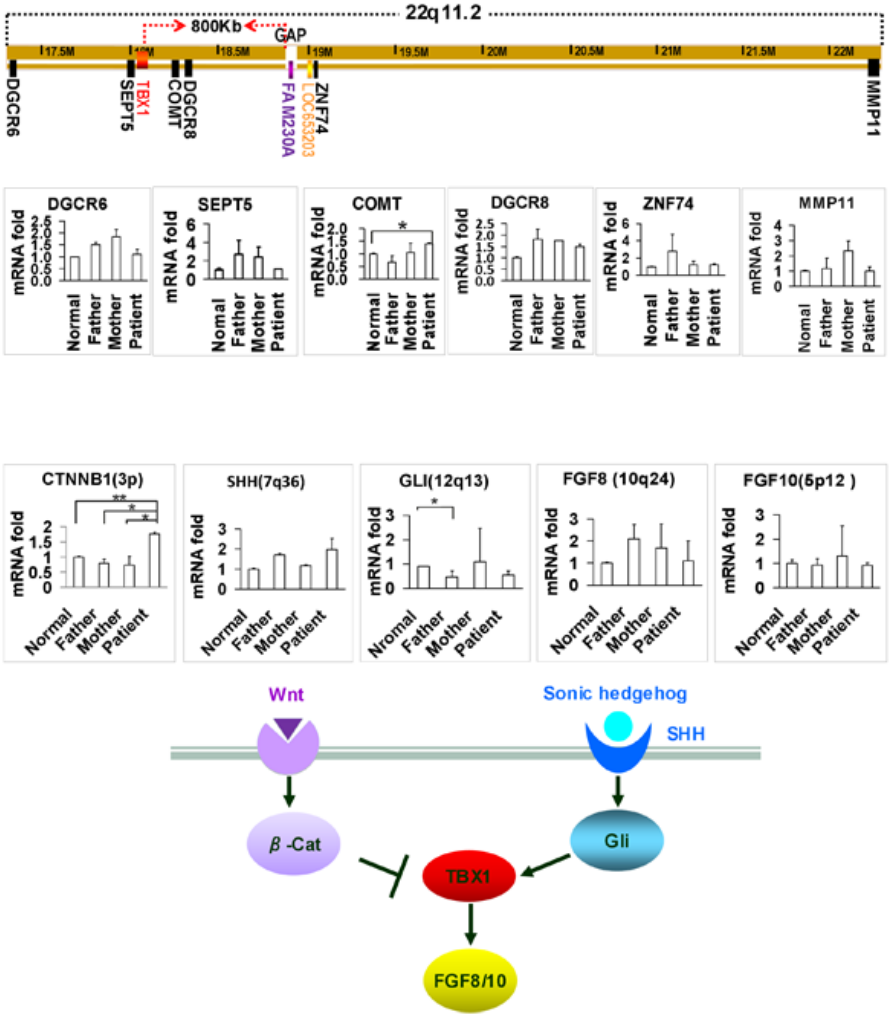

Supp. Figure S13. Expression of selected genes on chromosome 22 and genes related to *TBX1*. QRT-PCR showed no reduced expression of genes in the 3 Mb DGCR on chromosome 22 (*DGCR6*, *SEPT5*, *COMT*, *DGCR8*, *ZNF74*, and *MMP11*), a putative upstream regulator of TBX1 (*SHH*, *GLI)* and *TBX1* related genes (*FGF8 and FGF10*). Beta-catenin (*CTNNB1*) had significantly increased expression in the cells from the patient.

Supp. Table S1. Results of FISH Analysis

Probes	Localization**	Chromosomes[1]			
		9	der(9)	22	der(22)
LSI P16	**Chr9: 21792942-21995210**	+	+	−	+
VCFS	Chr22:17692778-17793773	−	−	+	+
RP11-1057H19	Chr22:17685254-17859197	−	−	+	+
TBX1	Chr22:18068734-18298734	−	−	+	+
RP11-138C22	Chr22:18253741-18429812	−	−	+	+
CTD-3148D21	Chr22:18439142-18578058	−	−	+	+
RP11-586I18	**Chr22:18853727-18976359**	**−**	**+**	**+**	**+**
CTD-3090o16	**Chr22:18879542-19020147**	**−**	**+**	**+**	**+**
RP11-562F10	**Chr22:19022375-19204954**	**−**	**+**	**+**	**+**
RP11-278E23	Chr22:19862624-19958793	−	−	+	+

[1]localized on indicated chromosome +, not-localized –, **BOLD type** = probes split by translocation

**UCSC May 2004 (NCBI35/hg17)

Supp. Table S2. Primers for the PCR amplification of chimeric genomic DNA and cDNA

Primer	Sequence (5'-3') **	PCR Product Length (bp)	Location on chromosomes
Genomic primers			
Chr9-1F	CTGATGCGGCATTGTAGGAT	2001	9
Chr9-1R	GGAGAAAGAAACATCCAATG		9
Chr9-2F	TAAATATAGCTTGGTGTTAAAAACAAAATATAC	660	9
Chr9-2R	TTGAGACGGAGTCTCGCTCT		9
Chr9-3F	AGTAGACAAATAAGTTACTTTTATTAGAATCA	400	9
Chr9-3R	TGCAAGCTCCGCCCCCCGGGTTCACGCCA		9
Chr9-4F	TCAGGCACTCGGCTTAAAGT	244	9
Chr9-4R	TTGAGACGGAGTCTCGCTCT		9
Chr9-5F	CTCCGTCTCAAAAAAAAAAA	311	9
Chr9-5R	AGTAGGTGGTAGAACTAGGACA		9
Chr9-6F	TACAAAAAATTAGCCAGGCG	626	9
Chr9-6R	CAGGGCATATATCTCGCTCT		9
Chr9-7F	CCCTGTCCTAGTTCTACCACC	383	9
Chr9-7R	GAGATCTACTCCCAGGGACAC		9
Der9-1F	GAGCACTTAGCTCCTGCAGAG	1162	22
Der9-1R	CTGGGAGCTCCATTACAGGG		9
Der9-2F	GCACTTAGCTCCTGCAGAGAG	1160	22
Der9-2R	CTGGGAGCTCCATTACAGGG		9
Der9-3F	TGGAGGGTATAGGGTTCTGCC	1443	22
Der9-3R	ATGCATCACCCCAGTCTTCCC		9
Der9-4F	GGAGGGTATAGGGTTCTGCC	1438	22
Der9-4R	ATCACCCCAGTCTTCCCTCC		9
Der9-5F	GCAGACTTGCACACAGACCAC	2660	22
Der9-5R	ATGCATCACCCCAGTCTTCCC		9
Der9-6F	GTCAGGCATAGTGGCTCACAC	1020	22
Der9-6R	TCCTTCAACGTTCCATCCCCC		9
Der9-7F	CTCAACCCCGCTGAGTGAAG	1762	22
Der9-7R	AGCCCACATGCCAGATGGAG		22
Der9-8F	GCTTGTTCAGGCCAGCCAAC	11699	9
Der9-8R	GGCTCCACTCAAGAGCTCATC		22
Der9-9F	TCAGGCCAGCCAACATACGAC	11691	9
Der9-9R	CTCCACTCAAGAGCTCATCCC		22
Der9-10F	CTGTCACTGCAGTTATTATGTGTTTTAG	12031	9
Der9-10R	AAGTGTGAGGTGTCATTTATCAGAAT		22
22a	GGTGTAGTCCCAGTGTGAATTGGGATTCAG		22
22b	CTGCATCCTTCAACGTTCCATC		22
22c	CCTCCAACGGATCCATACTACTG		22
22d	GTTGGGTGATTGACTGTGATTGAC		22
Der22-1F	TCCGAAGGCTGAGGAAGGAG	1240	9
Der22-1R	TCCTGCCCTTGGTCCTAAGT		22
Der22-2F	TCCGAAGGCTGAGGAAGGAG	1239	9
Der22-2R	CCTGCCCTTGGTCCTAAGTG		22
Der22-3F	CTGAGGAAGGAGAATGGCGTG	1232	9
Der22-3R	TCCTGCCCTTGGTCCTAAGTG		22
Der22-4F	AACAGAGCGAGACTCCGTCTC	1149	9
Der22-4R	TGCCCTTGGTCCTAAGTGCC		22
Der22-5F	TCCTTCAACGTTCCATCCCCC	899	22
Der22-5R	TGCCCTTGGTCCTAAGTGCC		22
Der22-6F	TTATGGCATCCTTGGGTGGGG	4037	9
Der22-6R	TCCTGCCCTTGGTCCTAAGTG		22
cDNA primers			
Qp14-1F	CGCGAGTGAGGGTTTTCGTG	100	9
Qp14-1R	TCAGTAGCATCAGCACGAGGG		9
DGCR15 cDNA-1F	ATGGGGAACCTGTGTGGCTG	105	22
DGCR15 cDNA-1R	GTGCTCCCTGAAGTCACCTTG		22

DGCR15 cDNA-2F	AGGAAGCCCTACTCTACCACC	106	22
DGCR15 cDNA-2R	GGAGCCATGAGGTCTCCTAC		22
DGCR15 cDNA-3F	GTGCACACCAACCAGTGTAGG	47	22
DGCR15 cDNA-3R	TCTTTACCCGGGAGCCATGAG		22
DGCR15 cDNA-4F	AGGAAGCCCTACTCTACCACC	198	22
DGCR15 cDNA-4R	AGAGTGGGCTGAAGCTTGTCC		22
DGCR15 cDNA-5F	GTGCACACCAACCAGTGTAGG	309	22
DGCR15 cDNA-5R	ACGGCGTCCTCGTTAGTGATG		22
DGCR15 cDNA-6F	ATGGGGAACCTGTGTGGCTG	441	22
DGCR15 cDNA-6R	ACGGCGTCCTCGTTAGTGATG		22
DGCR15 cDNA-7F	GTGCACACCAACCAGTGTAGG	546	22
DGCR15 cDNA-7R	ACCTCGTTAGCGATGCCGTG		22

F – forward primer
R – reverse primer

**GenBank version: Chr9-1 to Chr9-7: NT_008413.17/GI:89029256
Der9-1-10 and Der22-1-6: AC074203.3/GI:9625348 (on chr22) and AB060808.1/GI:20330501 (on chr9)
22a to 22c: AB334267.1/GI:158635835
FAM230A cDNA-1-7: NC_000022.10/GI:224589814

Supp. Table S3. Clinical and laboratory abnormalities in patient DD129BE

Clinical & Laboratory Abnormalities	Patient's Clinical Features Found In / Or Resembling DiGeorge Syndrome
Growth	Short stature
Face	Mild micronathia
Eyes	Myopia; Eyelid hooding
Hearing & Ear Structure	Simple, low set, posteriorly rotated ears; Profound sensorineural hearing loss; Abnormally folded pinnae; bilateral incomplete partition of the cochlea; hypoplasia of the lateral semicircular canals and vestibules; diminished or absent ostea for the VIIIth cranial nerves bilaterally
Nose	Prominent tubular nose; bulbous nasal tip; short philthrum
Mouth & Palatal Abnormalities	Narrow arched palate with dental crowding; small mouth
Heart	Bicuspid aortic valve; Mildly dilated aortic root
Urogenital	Shawl scrotum; bilateral inguinal hernias
Skeletal	Sandal toe deformity and overriding small toe; arthrogryposis; 5th finger clinodactaly
Immunology	Asthma; multiple ear infections; zoster age 14
Chromosome 22 DiGeorge Critical Region	9,22 Translocation
TBX1	Low expression

Supp. Table S4. Translocations on PATRR22

Translocation	Disorder	Partner sequence	Translocation type	References
t(1;22)(p22;q11.2)	ependymoma	AT-rich	Non-recurrent	(Gotter et al., 2004)
t(4;22) (q12;q11.2)	large B-cell lymphoma/ myeloproliferative	Non-AT-rich palindromic sequence	Non-recurrent	(Nimmakayalu et al., 2003)
t(8;22)(q24.13;q11.21)	dysgerminoma	AT-rich site	Non-recurrent	(Gotter et al., 2007; Gimelli et al., 2009; Sheridan et al., 2010)
t(9;22)(p21;q11.2)	DGS/melanoma	AT-rich site	Non-recurrent	This study
t(11;22)(q23;q11)	Unbalanced offspring with supernumerary der22 syndrome	PATRR11	Recurrent	(Kurahashi et al., 2000; Kurahashi and Emanuel, 2001a; Kurahashi et al., 2007)
t(17;22)(q11.2;q11.2)	neurofibromatosis type 1	PATRR17	Recurrent	(Ledbetter et al., 1989; Kehrer-Sawatzki et al., 1997; Kurahashi et al., 2003)